Solving the Payne-Whitham traffic flow model as a hyperbolic system of conservation laws with relaxation

W.L. Jin and H.M. Zhang*

August 30, 2001

Abstract: In this paper, we study the Payne-Whitham (PW) model as a hyperbolic system of conservation laws with relaxation. After studying the Riemann problem for the homogeneous version of the PW model, we introduce three first-order numerical solution methods for solving the system. In these methods, the homogeneous part of the PW model is approximated by Godunov-type difference equations, and different treatments of the source term are used. Numerical results show that solutions of the PW model with these methods are close to those of the LWR model when the PW model is stable, and that the PW model can simulate cluster effect in traffic when it is unstable. The PW model is also studied for roadways with inhomogeneities.

Keywords: The Payne-Whitham (PW) model, hyperbolic system of conservation laws with relaxation, Riemann problem, Godunov's method.

1 Introduction

Continuum models of vehicular traffic on long crowded roads have been studied and applied in simulation for decades. In these models, traffic conditions at a location x and time t are measured by density ρ, travel speed v, and flow-rate q, for which a basic relationship is that $q = \rho v$ at any location and any time. Traffic conservation, a principle governing the evolution of traffic conditions, can be described by a partial differential equation,

$$\rho_t + q_x \quad = \quad 0. \tag{1}$$

In the first continuum model by Lighthill and Whitham (1955) and Richards (1956), the LWR model, traffic is restricted to equilibrium states. That is, in the LWR model, q observes the equilibrium relation $q = f_*(\rho)$, which is also known as the fundamental diagram of traffic flow. Correspondingly, we have the speed-density relationship $v = v_*(\rho) \equiv f_*(\rho)/\rho$. Hence the LWR model can be written as

$$\rho_t + (\rho v_*(\rho))_x \quad = \quad 0. \tag{2}$$

Generally, the equilibrium velocity is assumed to be decreasing with respect to density; i.e., $v_*{}'(\rho) < 0$; the fundamental diagram is concave; i.e., $f_*''(\rho) < 0$.

*University of California, Davis, 95616

In reality, however, traffic is generally observed in nonequilibrium. Nonequilibrium traffic flow models are therefore suggested. Among them, the Payne-Whitham (PW) model (Payne, 1971; Whitham, 1974) is perhaps the best known. In the PW model, besides equation (1), a second equation, which defines traffic acceleration, is introduced,

$$v_t + vv_x + \frac{c_0^2}{\rho}\rho_x = \frac{v_*(\rho) - v}{\tau}, \tag{3}$$

where the constant $c_0 > 0$ is the traffic sound speed and τ the relaxation time.

With $q = \rho v$, the PW model can be written as

$$\begin{pmatrix} \rho \\ q \end{pmatrix}_t + \begin{pmatrix} q \\ \frac{q^2}{\rho} + c_0^2\rho \end{pmatrix}_x = \begin{pmatrix} 0 \\ \frac{f_*(\rho)-q}{\tau} \end{pmatrix}, \tag{4}$$

which is in the conservative form

$$u_t + f(u)_x = s(u), \tag{5}$$

where $u = (\rho, q)$ is the state variable. Thus the PW model is a "hyperbolic system of conservation laws with relaxation" in the sense of Whitham (1959; 1974) and Liu (1987). Schochet (1988) has shown that, as $\tau \to 0$, the system (4) admits the limit $\rho_t + (\rho v_*)_x = \nu\rho_{xx}$, which is the viscous version of the LWR model. Therefore the LWR model is called the degenerate system or subsystem of the PW model.

The system (4) has two wave speeds, called "frozen characteristic speeds" by Pember (1993), $\lambda_{1,2}(\rho, v) = v \mp c_0$. Since $v \geq 0$ and $c_0 > 0$, $\lambda_1 < \lambda_2$ and $\lambda_2 > 0$. Besides, the PW model has a sub-characteristic, $\lambda_*(\rho) = v_*(\rho) + \rho v_*'(\rho)$, which is the wave speed of the LWR model, can be positive or negative, and smaller than λ_2.

Whitham (1974) showed that the stability condition for the linearized system with a relaxation term is

$$\lambda_1 < \lambda_* < \lambda_2. \tag{6}$$

Liu (1987) showed that if the condition (6) is always satisfied, then the corresponding PW model is stable under small perturbations and the time-asymptotic solutions of system (4) are completely determined by the equilibrium LWR model. Chen, Levermore, and Liu (1994) showed that if condition (6) is satisfied, then solutions of the system tend to solutions of the equilibrium equations as the relaxation time tends to zero. Note that, since $\lambda_* < \lambda_2$ for the PW model, instability can only occur when $\lambda_1 < \lambda_*$ is violated (Zhang, 1999).

For solving the PW model numerically, Leo and Pretty (1992) applied Roe's flux difference splitting algorithm, in which an approximate Riemann solver is used. In this paper, we will study the PW model as a hyperbolic system of conservation laws with relaxation. In our study, the Riemann problem for the homogeneous version of the PW model is solved exactly. Based on this, we apply the Godunov methods, which are well-developed in the area of computational fluid dynamics, for finding the numerical solutions of the PW model. These methods can also be directly applied for the PW model of traffic on roadways with inhomogeneities, such as lane-drops.

The remaining part of this paper is organized as follows. In Section 2, we analytically solve the homogeneous version of the PW model. In Section 3, we study several different Godunov methods for the PW model. In Section 4, we present numerical results for the PW model with stable or unstable initial conditions and for a roadway with lane-drops. In Section 5, we conclude this paper with our findings of the numerical methods and the properties of the PW model.

2 Solving the homogeneous version of the PW model

The homogeneous version of the PW model can be written as

$$\begin{pmatrix} \rho \\ q \end{pmatrix}_t + \begin{pmatrix} q \\ \frac{q^2}{\rho} + c_0^2 \rho \end{pmatrix}_x = 0, \tag{7}$$

or

$$u_t + f(u)_x \quad = \quad 0, \tag{8}$$

which is a hyperbolic system of conservation laws. For (8), the Jacobian matrix can be written as $\partial f = \begin{pmatrix} 0 & 1 \\ -\frac{q^2}{\rho^2} + c_0^2 & 2\frac{q}{\rho} \end{pmatrix}$, for which the two real distinct eigenvalues are $\lambda_{1,2} = v \mp c_0$, and the corresponding right eigenvectors are

$$r_1 = (1, \lambda_1), \qquad r_2 = (1, \lambda_2).$$

Furthermore, the system (8) is genuinely nonlinear since

$$\nabla \lambda_i \cdot r_i \quad = \quad \mp \frac{c_0}{\rho} \neq 0.$$

Discussions of general hyperbolic systems of conservation laws can be found in (Smoller, 1983). Here we follow discussions by Zhang (1998, 1999, 2000, 2001), which are carried out for a model similar to the PW model.

2.1 The Riemann problem

The Riemann problem for (8) around $x = 0$ has the following jump initial conditions:

$$u(x, t = 0) \quad = \quad \begin{cases} u_l = (\rho_l, q_l), & \text{if } x < 0, \\ u_r = (\rho_r, q_r), & \text{if } x > 0. \end{cases} \tag{9}$$

This problem is solved by shock waves and/or rarefaction waves.

We begin by studying shock waves. As we know, there are two distinct types of shock waves for (8); namely, 1-shocks and 2-shocks. Lax's (1972) entropy condition states that 1-shocks satisfy

$$\lambda_1(u_r) < s < \lambda_1(u_l), \qquad s < \lambda_2(u_r), \tag{10}$$

and 2-shocks satisfy

$$\lambda_2(u_r) < s < \lambda_2(u_l), \qquad s > \lambda_1(u_l). \tag{11}$$

In both (10) and (11), the shock wave speed s is determined by the Rankine-Hugoniot jump condition

$$\begin{aligned} s[\rho] &= [q], \\ s[q] &= \left[\frac{q^2}{\rho} + c_0^2\rho\right]. \end{aligned}$$

These two equations yield

$$\frac{q_r}{\rho_r} - \frac{q_l}{\rho_l} = \pm c_0 \frac{\rho_r - \rho_l}{\sqrt{\rho_r \rho_l}}. \tag{12}$$

For 1-shocks, the first inequality of (10) yields

$$\frac{q_r}{\rho_r} - c_0 < s = \frac{q_r - q_l}{\rho_r - \rho_l} < \frac{q_l}{\rho_l} - c_0,$$

or

$$\frac{q_r}{\rho_r} - \frac{q_r - q_l}{\rho_r - \rho_l} - c_0 < 0 < \frac{q_l}{\rho_l} - \frac{q_r - q_l}{\rho_r - \rho_l} - c_0,$$

hence

$$\frac{\rho_r q_l - \rho_l q_r}{\rho_r - \rho_l}\Big/\rho_r - c_0 < 0 < \frac{\rho_r q_l - \rho_l q_r}{\rho_r - \rho_l}\Big/\rho_l - c_0.$$

Since $c_0, \rho_l > 0$, we obtain

$$c_0\rho_r > \frac{\rho_r q_l - \rho_l q_r}{\rho_r - \rho_l} > c_0\rho_l > 0.$$

Hence

$$\rho_l < \rho_r, \qquad \frac{q_l}{\rho_l} > \frac{q_r}{\rho_r}. \tag{13}$$

Moreover,

$$\begin{aligned} s - \lambda_2(u_r) &= \frac{q_r - q_l}{\rho_r - \rho_l} - \frac{q_r}{\rho_r} - c_0 \\ &= \frac{\rho_l q_r - \rho_r q_l}{(\rho_r - \rho_l)\rho_r} - c_0 < -c_0 < 0; \end{aligned}$$

i.e., if u_l and u_r satisfy (13), then they also satisfy the second part of the entropy condition (10). Therefore, the states which can be connected to u_l by a 1-shock on the right must lie on the curve (denoted by S_1)

$$S_1: \quad \frac{q}{\rho} - \frac{q_l}{\rho_l} = -c_0 \frac{\rho - \rho_l}{\sqrt{\rho\rho_l}} \equiv s_1(\rho; u_l), \quad \rho > \rho_l,\ \frac{q}{\rho} < \frac{q_l}{\rho_l}. \tag{14}$$

Finally, by direct calculations, we find

$$\frac{ds_1}{d\rho} = -\frac{c_0(\rho+\rho_l)}{2\rho\sqrt{\rho\rho_l}} < 0, \qquad \frac{d^2s_1}{d\rho^2} = \frac{c_0(\rho+3\rho_l)}{4\rho^2\sqrt{\rho\rho_l}} > 0;$$

i.e., S_1 is decreasing and convex.

With similar analyses, we obtain the curve (denoted by S_2) consisting of those states which can be connected to u_l by a 2-shock on the right

$$S_2: \quad \frac{q}{\rho} - \frac{q_l}{\rho_l} = c_0\frac{\rho-\rho_l}{\sqrt{\rho\rho_l}} \equiv s_2(\rho; u_l), \quad \rho < \rho_l,\ \frac{q}{\rho} < \frac{q_l}{\rho_l}, \tag{15}$$

and

$$\frac{ds_2}{d\rho} = \frac{c_0(\rho+\rho_l)}{2\rho\sqrt{\rho\rho_l}} > 0, \qquad \frac{d^2s_2}{d\rho^2} = -\frac{c_0(\rho+3\rho_l)}{4\rho^2\sqrt{\rho\rho_l}} < 0.$$

Besides shock wave solutions, the Riemann problem for (8) admits two families of rarefaction waves, which are continuous in the form $u(x,t) = u(x/t)$ and satisfy that $\lambda_i(u(x/t))$ increases as x/t increases. Let $\xi = x/t$, $u(x,t) = u(\xi)$ satisfies the following ordinary differential equation,

$$-\xi u_\xi + \partial f u_\xi = 0,$$

or

$$(\partial f - \xi I)u_\xi = 0.$$

If $u_\xi \neq 0$, then ξ is the eigenvalue for ∂f and $u_\xi = (\rho_\xi, q_\xi)$ is the corresponding eigenvector. Related to the two real and distinct eigenvalues $\lambda_{1,2}$ of ∂f, there exist two families of rarefaction waves: 1-rarefaction waves and 2-rarefaction waves.

For 1-rarefaction waves, the eigenvector u_ξ satisfies

$$\begin{pmatrix} -\lambda_1 & 1 \\ -\frac{q^2}{\rho^2} + c_0^2 & 2\frac{q}{\rho} - \lambda_1 \end{pmatrix}\begin{pmatrix} \rho_\xi \\ q_\xi \end{pmatrix} = \begin{pmatrix} 0 \\ 0 \end{pmatrix},$$

which yields $-\lambda_1\rho_\xi + q_\xi = 0$. Since $\rho_\xi \neq 0$, we obtain $q_\xi/\rho_\xi = \lambda_1$. Hence,

$$\frac{dq}{d\rho} = \lambda_1 = \frac{q}{\rho} - c_0.$$

Solving this equation, we obtain the 1-rarefaction wave curve

$$R_1: \quad \frac{q}{\rho} - \frac{q_l}{\rho_l} = -c_0\ln(\rho/\rho_l) \equiv r_1(\rho; u_l). \tag{16}$$

Here R_1 is the curve consisting of states which can be connected to u_l by a 1-rarefaction wave on the right. Since $\lambda_1(u) > \lambda_1(u_l)$, the states on this curve must satisfy $q/\rho > q_l/\rho_l$, and, from (16), we have $\rho < \rho_l$. We can also find

$$\frac{dr_1}{d\rho} = -\frac{c_0}{\rho} < 0, \text{ and } \frac{d^2r_1}{d\rho^2} = \frac{c_0}{\rho^2} > 0.$$

Similarly we obtain the 2-rarefaction wave curve

$$R_2: \quad \frac{q}{\rho} - \frac{q_l}{\rho_l} \;=\; c_0 \ln(\rho/\rho_l) \equiv r_2(\rho; u_l), \quad \rho > \rho_l,\ \frac{q}{\rho} > \frac{q_l}{\rho_l}, \tag{17}$$

and

$$\frac{dr_2}{d\rho} = \frac{c_0}{\rho} > 0, \text{ and } \frac{d^2 r_2}{d\rho^2} = -\frac{c_0}{\rho^2} < 0.$$

The four basic types of wave solutions are depicted in **Figure** 1. From the figure we can see that the state space is partitioned into four regions, and, when u_r locates in each of these regions, the Riemann problem is solved by a wave combining two basic waves. Totally, therefore, there are eight types of wave solutions to the Riemann problem, including 1-shock waves (S_1), 2-shock waves (S_2), 1-rarefaction waves (R_1), 2-rarefaction waves (R_2), S_1-S_2 (left S_1 and right S_2) waves, R_1-R_2 (left R_1 and right R_2) waves, R_1-S_2 (left R_1 and right S_2) waves, and S_1-R_2 (left S_1 and right R_2) waves. These wave solutions are self-similar in the sense that $u(x/t)$ is constant when x/t=const. Note that the curves S_1 and R_1 have a second-order contact at u_l; i.e., their first two derivatives are equal at this point, and the same is true for the two corresponding curves in the second characteristic family.

2.2 The time average of u at $x = 0$

In this subsection, we compute the averages of ρ and q at the boundary $x = 0$ over a time interval $(0, \Delta t)$ from the Riemann solutions for (8) with initial data (u_l, u_r). These averages, denoted by ρ_0^* and q_0^*, are defined by

$$\rho_0^* = \frac{1}{\Delta t}\int_0^{\Delta t} \rho(x = 0, t)\mathrm{dt} \quad \text{and} \quad q_0^* = \frac{1}{\Delta t}\int_0^{\Delta t} q(x = 0, t)\mathrm{dt}.$$

As we know, the Riemann problem has eight types of self-similar wave solutions. Therefore the time average (ρ_0^*, q_0^*) is equal to the boundary state $u(x = 0, t > 0)$, which is a constant. For the eight types of wave solutions, conditions of their existence and the corresponding boundary states (ρ_0^*, q_0^*) are discussed one by one as follows.

1. S_1 – If (u_l, u_r) satisfy

$$S_1: \quad \frac{q_r}{\rho_r} - \frac{q_l}{\rho_l} \;=\; -c_0\frac{\rho_r - \rho_l}{\sqrt{\rho_r \rho_l}}, \quad \rho_r > \rho_l,\ \frac{q_r}{\rho_r} < \frac{q_l}{\rho_l},$$

the Riemann problem for (8) with initial data (u_l, u_r) is solved by a 1-shock, and the shock speed is

$$s \;=\; \frac{q_r - q_l}{\rho_r - \rho_l}.$$

For S_1-type solutions, (ρ_0^*, q_0^*) is summarized in **Table** 1.

S_1	$s = \frac{q_r - q_l}{\rho_r - \rho_l}$	ρ_0^*	q_0^*
	$s > 0$	ρ_l	q_l
	$s \leq 0$	ρ_r	q_r

Table 1: The boundary state for S_1-type solutions

S_2	$s = \frac{q_r - q_l}{\rho_r - \rho_l}$	ρ_0^*	q_0^*
	$s > 0$	ρ_l	q_l

Table 2: The boundary state for S_2-type solutions

2. S_2 – If (u_l, u_r) satisfy

$$S_2: \quad \frac{q_r}{\rho_r} - \frac{q_l}{\rho_l} = c_0 \frac{\rho_r - \rho_l}{\sqrt{\rho_r \rho_l}}, \quad \rho_r < \rho_l, \ \frac{q_r}{\rho_r} < \frac{q_l}{\rho_l},$$

the Riemann problem for (8) with initial data (u_l, u_r) is solved by a 2-shock. Since the wave speed

$$s = \frac{q_r - q_l}{\rho_r - \rho_l} > 0,$$

(ρ_0^*, q_0^*) for this type of solutions is the same as (ρ_l, q_l) and shown in **Table** 2.

3. R_1 – If (u_l, u_r) satisfy

$$R_1: \quad \frac{q_r}{\rho_r} - \frac{q_l}{\rho_l} = -c_0 \ln(\rho_r/\rho_l) \quad \rho_r < \rho_l, \ \frac{q_r}{\rho_r} > \frac{q_l}{\rho_l},$$

the Riemann problem for (8) with initial data (u_l, u_r) is solved by a 1-rarefaction, and the characteristic velocity is determined by the first eigenvalue of the system:

$$\lambda_1(\rho, q) = \frac{q}{\rho} - c_0.$$

If $\lambda_1(u_l) \geq 0$, the boundary state $(\rho_0^*,\ q_0^*)$ is the same as the left state, i.e., $(\rho_l,\ q_l)$; similarly, if $\lambda_1(u_r) \leq 0$, it is the right state; otherwise, (ρ_0^*, q_0^*) solves the following equations:

$$\begin{aligned} \lambda_1(\rho_0^*, q_0^*) &= \frac{q_0^*}{\rho_0^*} - c_0 = 0, \\ \frac{q_0^*}{\rho_0^*} - \frac{q_l}{\rho_l} &= -c_0 \ln(\rho_0^*/\rho_l). \end{aligned}$$

Solving them we obtain

$$\rho_0^* = \rho_l e^{-1 + q_l/(c_0 \rho_l)}, \tag{18}$$

$$q_0^* = c_0 \rho_0^*. \tag{19}$$

For this type of solutions, (ρ_0^*, q_0^*) is summarized in **Table** 3.

R_1	λ_1	ρ_0^*	q_0^*
	$\lambda_1(u_l) \geq 0$	ρ_l	q_l
	$\lambda_1(u_r) \leq 0$	ρ_r	q_r
	o.w.	given in (18) and (19)	

Table 3: The boundary state for R_1-type solutions

	λ_2	ρ_0^*	q_0^*
R_2	$\lambda_2 > 0$	ρ_l	q_l

Table 4: The boundary state for R_2-type solutions

4. R_2 – If (u_l, u_r) satisfy

$$R_2: \quad \frac{q_r}{\rho_r} - \frac{q_l}{\rho_l} = c_0 \ln(\rho_r/\rho_l), \quad \rho_r > \rho_l, \ \frac{q_r}{\rho_r} > \frac{q_l}{\rho_l},$$

the Riemann problem for (8) with initial data (u_l, u_r) is solved by a 2-rarefaction. Since the characteristic velocity, i.e., the second eigenvalue of the system, is $\lambda_2(\rho, q) = q/\rho + c_0 > 0$, (ρ_0^*, q_0^*) for this type of solutions is the same as the left state and shown in **Table** 4.

5. R_1-R_2 – If (u_l, u_r) satisfy

$$R_1: \quad \frac{q_m}{\rho_m} - \frac{q_l}{\rho_l} = -c_0 \ln(\rho_m/\rho_l), \quad \rho_m < \rho_l, \ \frac{q_m}{\rho_m} > \frac{q_l}{\rho_l}, \tag{20}$$

and

$$R_2: \quad \frac{q_r}{\rho_r} - \frac{q_m}{\rho_m} = c_0 \ln(\rho_r/\rho_m), \quad \rho_r > \rho_m, \ \frac{q_r}{\rho_r} > \frac{q_m}{\rho_m}, \tag{21}$$

where $u_m = (\rho_m, q_m)$ is an intermediate state, the Riemann problem for (8) with initial data (u_l, u_r) is solved by a 1-rarefaction + 2-rarefaction wave. Adding (20) to (21), we find

$$-c_0 \ln \frac{\rho_m^2}{\rho_l \rho_r} = \frac{q_r}{\rho_r} - \frac{q_l}{\rho_l},$$

hence

$$\rho_m = \sqrt{\rho_l \rho_r} e^{-\frac{q_r/\rho_r - q_l/\rho_l}{2c_0}},$$

where $\rho_m < \rho_l$ and $\rho_m < \rho_r$, and

$$q_m = q_l \rho_m/\rho_l - c_0 \rho_m \ln(\rho_m/\rho_l).$$

Note that (ρ_0^*, q_0^*) is only related to the 1-rarefaction wave connecting u_l and u_m. Therefore, the boundary state is summarized in **Table** 5.

R_1-R_2	λ_1	ρ_0^*	q_0^*
	$\lambda_1(u_l) \geq 0$	ρ_l	q_l
	$\lambda_1(u_m) \leq 0$	ρ_m	q_m
	o.w.	given in (18) and (19)	

Table 5: The boundary state for R_1-R_2-type solutions

R_1-S_2	λ_1	ρ_0^*	q_0^*
	$\lambda_1(u_l) \geq 0$	ρ_l	q_l
	$\lambda_1(u_m) \leq 0$	ρ_m	q_m
	o.w.	given in (18) and (19)	

Table 6: The boundary state for R_1-S_2-type solutions

6. R_1-S_2 – If (u_l, u_r) satisfy

$$R_1: \quad \frac{q_m}{\rho_m} - \frac{q_l}{\rho_l} = -c_0 \ln(\rho_m/\rho_l), \quad \rho_m < \rho_l, \ \frac{q_m}{\rho_m} > \frac{q_l}{\rho_l},$$

and

$$S_2: \quad \frac{q_r}{\rho_r} - \frac{q_m}{\rho_m} = c_0 \frac{\rho_r - \rho_m}{\sqrt{\rho_r \rho_m}}, \quad \rho_r < \rho_m, \ \frac{q_r}{\rho_r} < \frac{q_m}{\rho_m},$$

where $u_m = (\rho_m, q_m)$ is an intermediate state, the Riemann problem for (8) with initial data (u_l, u_r) is solved by a 1-rarefaction+2-shock wave. These two equations yield

$$c_0 \ln(\rho_m/\rho_l) - c_0 \frac{\rho_r - \rho_m}{\sqrt{\rho_r \rho_m}} + \frac{q_r}{\rho_r} - \frac{q_l}{\rho_l} = 0, \tag{22}$$

where $\rho_r < \rho_m < \rho_l$. From (22) we can obtain ρ_m and then compute q_m as follows

$$q_m = q_l \rho_m/\rho_l - c_0 \rho_m \ln(\rho_m/\rho_l).$$

Hence, (ρ_0^*, q_0^*) can be determined from the 1-rarefaction wave connecting u_l and u_m and is summarized in **Table** 6.

7. S_1-S_2 – If (u_l, u_r) satisfy

$$S_1: \quad \frac{q_m}{\rho_m} - \frac{q_l}{\rho_l} = -c_0 \frac{\rho_m - \rho_l}{\sqrt{\rho_m \rho_l}}, \quad \rho_m > \rho_l, \ \frac{q_m}{\rho_m} < \frac{q_l}{\rho_l},$$

and

$$S_2: \quad \frac{q_r}{\rho_r} - \frac{q_m}{\rho_m} = c_0 \frac{\rho_r - \rho_m}{\sqrt{\rho_r \rho_m}}, \quad \rho_r < \rho_m, \ \frac{q_r}{\rho_r} < \frac{q_m}{\rho_m},$$

S_1-S_2	$s = \frac{q_m - q_l}{\rho_m - \rho_l}$	ρ_0^*	q_0^*
	$s > 0$	ρ_l	q_l
	$s \leq 0$	ρ_m	q_m

Table 7: The boundary state for S_1-S_2-type solutions

where $u_m = (\rho_m, q_m)$ is an intermediate state, the Riemann problem for (8) with initial data (u_l, u_r) is solved by a 1-shock+2-shock wave. These two equations yield

$$c_0 \frac{\rho_m - \rho_l}{\sqrt{\rho_m \rho_l}} - c_0 \frac{\rho_r - \rho_m}{\sqrt{\rho_r \rho_m}} + \frac{q_r}{\rho_r} - \frac{q_l}{\rho_l} = 0, \tag{23}$$

where $\rho_m > \rho_l$ and $\rho_m > \rho_r$. From (23) we can obtain ρ_m and then compute q_m as follows,

$$q_m = \rho_m \frac{q_l}{\rho_l} - c_0 \rho_m \frac{\rho_m - \rho_l}{\sqrt{\rho_m \rho_l}}.$$

Hence, (ρ_0^*, q_0^*) can be determined from the 1-shock connecting u_l and u_m and is summarized in **Table** 7.

8. S_1-R_2 – If (u_l, u_r) satisfy

$$S_1: \quad \frac{q_m}{\rho_m} - \frac{q_l}{\rho_l} = -c_0 \frac{\rho_m - \rho_l}{\sqrt{\rho_m \rho_l}}, \quad \rho_m > \rho_l, \ \frac{q_m}{\rho_m} < \frac{q_l}{\rho_l},$$

and

$$R_2: \quad \frac{q_r}{\rho_r} - \frac{q_m}{\rho_m} = c_0 \ln(\rho_r/\rho_m) \quad \rho_r > \rho_m, \ \frac{q_r}{\rho_r} > \frac{q_m}{\rho_m},$$

where $u_m = (\rho_m, q_m)$ is an intermediate state, the Riemann problem for (8) with initial data (u_l, u_r) is solved by a 1-shock+2-rarefaction wave. These two equations yield

$$c_0 \frac{\rho_m - \rho_l}{\sqrt{\rho_m \rho_l}} - c_0 \ln(\rho_r/\rho_m) + \frac{q_r}{\rho_r} - \frac{q_l}{\rho_l} = 0, \tag{24}$$

where $\rho_r > \rho_m > \rho_l$. From (24) we can obtain ρ_m and then compute q_m as follows,

$$q_m = \rho_m \frac{q_l}{\rho_l} - c_0 \rho_m \frac{\rho_m - \rho_l}{\sqrt{\rho_l \rho_m}}.$$

Hence, (ρ_0^*, q_0^*) can be determined from the 1-shock connecting u_l and u_m and is summarized in **Table** 8.

Remarks: For R_1-S_2-type solutions, (22) cannot be analytically solved to obtain ρ_m. Note that ρ_m is the solution of $f_6(\rho) = 0$, where (letting $\beta = (\frac{q_r}{\rho_r} - \frac{q_l}{\rho_l})/c_0$)

$$f_6(\rho) = \ln(\rho/\rho_l) - \frac{\rho_r - \rho}{\sqrt{\rho_r \rho}} + \beta, \quad \rho_l > \rho > \rho_r,$$

S_1-R_2	$s = \frac{q_m - q_l}{\rho_m - \rho_l}$	ρ_0^*	q_0^*
	$s > 0$	ρ_l	q_l
	$s \leq 0$	ρ_m	q_m

Table 8: The boundary state for S_1-R_2-type solutions

whose derivative is

$$f_6'(\rho) = \frac{1}{\rho} + \frac{\rho + \rho_r}{2\rho\sqrt{\rho\rho_r}} > 0.$$

Similarly, for S_1-S_2-type solutions, ρ_m is the solution of $f_7(\rho) = 0$, where

$$f_7(\rho) = \frac{\rho - \rho_l}{\sqrt{\rho\rho_l}} - \frac{\rho_r - \rho}{\sqrt{\rho_r\rho}} + \beta, \quad \rho > \rho_l, \rho_r,$$

and

$$f_7'(\rho) = \frac{\rho + \rho_l}{2\rho\sqrt{\rho\rho_l}} + \frac{\rho + \rho_r}{2\rho\sqrt{\rho\rho_r}} > 0;$$

and, for S_1-R_2-type solutions, ρ_m is the solution of $f_8(\rho) = 0$, where

$$f_8(\rho) = \frac{\rho - \rho_l}{\sqrt{\rho\rho_l}} - \ln(\rho_r/\rho) + \beta, \quad \rho_l < \rho < \rho_r,$$

and

$$f_8'(\rho) = \frac{\rho + \rho_l}{2\rho\sqrt{\rho\rho_l}} + \frac{1}{\rho} > 0.$$

To solve $f_i(\rho_m) = 0$ $(i = 6, 7, 8)$, therefore, we can apply Newton's method; i.e., given kth candidate ρ_k for ρ_m, $(k+1)$th candidate can be computed as

$$\rho_{k+1} = \rho_k - \frac{f_i(\rho_k)}{f_i'(\rho_k)}, \quad i = 6, 7, \text{ or } 8.$$

Also, for each type of solutions, ρ_{k+1} should be inside the given domain of ρ_m.

3 Numerical solution methods for the PW model

The Godunov (1959) method is efficient for solving hyperbolic systems of conservation laws. For the homogeneous version of the PW model, therefore, we will use the Godunov-type difference equations to approximate it. The PW model, however, has one relaxation term. Thus, different treatments of the effects of the source term result in different methods.

A general system (5) can be approximated by the following Godunov-type finite difference equation,

$$U_i^{j+1} = U_i^j - \frac{\Delta t}{\Delta x}(f(U_{i+1/2}^{*j}) - f(U_{i-1/2}^{*j})) + \Delta t \tilde{s}(u), \tag{25}$$

in which $U_i^j = (\rho_i^j, q_i^j)$ is the average of $u(x,t)$ over ith cell at time $j\Delta t$, $\tilde{s}(u)$ is the average of the source term over $((i-1/2)\Delta x, (i+1/2)\Delta x) \times (j\Delta t, (j+1)\Delta t)$, and the boundary state $U_{i+1/2}^{*j} = (\rho_{i+1/2}^{*j}, q_{i+1/2}^{*j})$ is computed, as shown in the preceding section, from the Riemann problem for (8) with initial condition

$$u_{i+1/2}(x, t_j) = \begin{cases} u_l, & \text{if } x - x_{i+1/2} < 0, \\ u_r, & \text{if } x - x_{i+1/2} \geq 0, \end{cases} \tag{26}$$

where $u_l = U_i^j$ and $u_r = U_i^{j+1}$.

When the source term is approximated implicitly, we call the numerical solution method as the implicit method. In this method, the PW model can be approximated by

$$\frac{\rho_i^{j+1} - \rho_i^j}{k} + \frac{q_{i+1/2}^{*j} - q_{i-1/2}^{*j}}{h} = 0, \tag{27}$$

$$\frac{q_i^{j+1} - q_i^j}{k} + \frac{\frac{{q_{i+1/2}^{*j}}^2}{\rho_{i+1/2}^{*j}} + c_0^2 \rho_{i+1/2}^{*j} - \frac{{q_{i-1/2}^{*j}}^2}{\rho_{i-1/2}^{*j}} - c_0^2 \rho_{i-1/2}^{*j}}{h} = \frac{f_*(\rho_i^{j+1}) - q_i^{j+1}}{\tau}, \tag{28}$$

from which we can write the evolution equations for the PW model as

$$\rho_i^{j+1} = \rho_i^j - \frac{k}{h}(q_{i+1/2}^{*j} - q_{i-1/2}^{*j}), \tag{29}$$

$$q_i^{j+1} = \frac{1}{(1+\frac{k}{\tau})} \left\{ q_i^j - \frac{k}{h} \left[\frac{{q_{i+1/2}^{*j}}^2}{\rho_{i+1/2}^{*j}} + c_0^2 \rho_{i+1/2}^{*j} - \frac{{q_{i-1/2}^{*j}}^2}{\rho_{i-1/2}^{*j}} - c_0^2 \rho_{i-1/2}^{*j} \right] + \frac{k}{\tau} f_*(\rho_i^{j+1}) \right\}. \tag{30}$$

Besides the implicit method, an explicit treatment was used for the source term in (Pember, 1993), where u is approximated by the averages of boundary states, and $\tilde{s}(u) = \frac{1}{2}(s(U_{i-1/2}^{*j}) + s(U_{i+1/2}^{*j}))$. Here the corresponding method is called the explicit method.

A third treatment of the source term is used in the fractional step splitting method, in which each time step Δt is split into three steps. In the first and third fractional steps, a first-order implicit method is used to integrate

$$\begin{pmatrix} \rho \\ q \end{pmatrix}_t = \begin{pmatrix} 0 \\ \frac{f_*(\rho) - q}{\tau} \end{pmatrix},$$

for time steps of $\Delta t/2$. In the second step, we solve the corresponding homogeneous system of (4) for a time step of Δt.

4 Numerical simulations of the PW model

In this section, we perform numerical simulations of the PW model for traffic on a ring road. The model parameters are chosen as follows (Kerner and Konhäuser, 1994; Herrman and Kerner, 1998): the unit length $l = 0.028$ km, the relaxation time $\tau = 5$ s, the free flow speed $v_f = 5l/\tau$, the jam density $\rho_j = 180$ veh/km, and the sound speed $c_0 = 2.48445l/\tau$; the equilibrium speed-density relationship $v_*(\rho) = 5.0461[(1 + \exp\{[\rho/\rho_j - 0.25]/0.06\})^{-1} - 3.72 \times 10^{-6}]l/\tau$. The equilibrium functions $v_*(\rho)$ and $f_*(\rho)$ are shown in **Figure** 2, in which the two critical densities $\rho_{c1} = 0.173\rho_j$=31 veh/km and $\rho_{c2} = 0.396\rho_j$=71 veh/km, determined by $\lambda_* = \lambda_1$, i.e., $\rho v_*'(\rho)+c_0 = 0$.

The length of the ring road is $L = 800l$ and the time interval $[0, T]$, where $T = 500\tau$. In the numerical studies, we partition the roadway into N cells and the time interval into K steps, with $N/K = 1/5$; e.g., if $N = 100$ and $K = 500$, the cell length is $\Delta x = 8l$ km and the length of each time step $\Delta t = 1\tau$ s. Since $\lambda_2 \le v_f + c_0 < 7.5l/\tau$, we find that the CFL (Courant, Friedrichs and Lewy, 1928) condition number $\lambda_2\Delta t/\Delta x \le 0.9375 < 1$.

4.1 Convergence rates for different methods when the PW model is stable

In this subsection, convergence rates for the three methods are computed by comparing solutions of the PW model, when it is stable, at time $T_0 = 500\tau$ for two different number of cells into which the roadway is partitioned, e.g., $2N$ and N. Denote solutions as $(U_i^{2N})_{i=1}^{2N}$ for $2N$ cells and $(U_i^N)_{i=1}^N$ for N cells respectively, and define a difference vector $(e^{2N-N})_{i=1}^N$ between these two solutions as

$$\mathbf{e}_i^{2N-N} = \frac{1}{2}(U_{2i-1}^{2N} + U_{2i}^{2N}) - U_i^N, i = 1, \cdots, N, \tag{31}$$

the relative error with respect to L^1-, L^2- or L^∞-norm can be computed as

$$\epsilon^{2N-N} = \| \mathbf{e}^{2N-N} \|. \tag{32}$$

Finally, the convergence rate r is obtained by comparing two relative errors:

$$r = \log_2(\frac{\epsilon^{2N-N}}{\epsilon^{4N-2N}}). \tag{33}$$

Here U can be ρ or v.

Here we use the following global perturbation as the initial traffic conditions:

$$\begin{aligned} \rho(x, 0) &= \rho_h + \Delta\rho_0 \sin(2\pi x/L), \quad x \in [0, L], \\ v(x, 0) &= v_*(\rho_h) + \Delta v_0 \sin(2\pi x/L), \quad x \in [0, L]. \end{aligned} \tag{34}$$

Setting $\rho_h = 20$ veh/km, $\Delta\rho_0 = 3$ veh/km, and $\Delta v_0 = 0.002$ km/s, the initial conditions are inside the stable region of the PW model.

Setting N=64, 128, 256, 512, and 1024, the relative errors and convergence rates for the implicit method, the explicit method, and the fractional step splitting method are respectively given in **Tables** 9, 10, and 11. From these tables, we can see that the convergence rates in the L^1 norm are close to one but lower in the L^2 and L^∞ norms, all rates increase with respect to N, and the fractional step splitting method has the highest convergence rates.

ρ	128-64	Rate	256-128	Rate	512-256	Rate	1024-512
L^1	1.95e-01	0.79	1.12e-01	0.88	6.12e-02	0.93	3.20e-02
L^2	2.57e-01	0.64	1.65e-01	0.76	9.78e-02	0.85	5.42e-02
L^∞	5.48e-01	0.37	4.24e-01	0.56	2.88e-01	0.73	1.74e-01
v	128-64	Rate	256-128	Rate	512-256	Rate	1024-512
L^1	4.21e-05	0.78	2.45e-05	0.87	1.34e-05	0.93	7.04e-06
L^2	5.61e-05	0.62	3.65e-05	0.74	2.19e-05	0.84	1.22e-05
L^∞	1.30e-04	0.35	1.02e-04	0.55	6.98e-05	0.72	4.25e-05

Table 9: Convergence rates for the implicit method

ρ	128-64	Rate	256-128	Rate	512-256	Rate	1024-512
L^1	2.06e-01	0.77	1.21e-01	0.87	6.64e-02	0.93	3.49e-02
L^2	2.67e-01	0.62	1.74e-01	0.74	1.04e-01	0.84	5.83e-02
L^∞	5.59e-01	0.34	4.42e-01	0.53	3.05e-01	0.70	1.88e-01
v	128-64	Rate	256-128	Rate	512-256	Rate	1024-512
L^1	4.46e-05	0.76	2.63e-05	0.86	1.45e-05	0.92	7.71e-06
L^2	5.82e-05	0.60	3.83e-05	0.72	2.32e-05	0.82	1.31e-05
L^∞	1.30e-04	0.32	1.04e-04	0.52	7.26e-05	0.69	4.50e-05

Table 10: Convergence rates for the explicit method

ρ	128-64	Rate	256-128	Rate	512-256	Rate	1024-512
L^1	1.81e-01	0.85	1.00e-01	0.92	5.31e-02	0.96	2.73e-02
L^2	2.43e-01	0.70	1.50e-01	0.81	8.58e-02	0.89	4.64e-02
L^∞	5.31e-01	0.42	3.96e-01	0.62	2.57e-01	0.77	1.51e-01
v	128-64	Rate	256-128	Rate	512-256	Rate	1024-512
L^1	3.91e-05	0.85	2.17e-05	0.92	1.15e-05	0.96	5.93e-06
L^2	5.30e-05	0.69	3.29e-05	0.80	1.89e-05	0.88	1.03e-05
L^∞	1.24e-04	0.43	9.23e-05	0.61	6.04e-05	0.77	3.55e-05

Table 11: Convergence rates for the fractional step splitting method

4.2 Comparison of solutions by different methods

Still using (34) as initial conditions and setting $N = 100$ and $K = 500$, we obtain solutions of the PW model with the implicit method, shown in **Figure** 3, from which we find that traffic approaches equilibrium after a sufficiently long time. Comparison of solutions at different times with different methods are shown in **Figure** 4, from which we can see that solutions by these methods are close to each other.

For the same fundamental diagram, initial ρ, N, and K, we solve the LWR model and obtain similar solutions as those of the PW model, as shown in **Figure** 5. The figure shows that, when the PW model is stable, it behaves similarly as the corresponding LWR model in large time.

4.3 Simulation of unstable traffic

Unstable phenomena, such as breakdowns and vehicle clusters, can be often observed in traffic flow. The PW model is capable of simulating unstable traffic under unstable initial traffic conditions, which can be seen from the following example.

For initial conditions (34) when $\rho_h = 33$ veh/km, $\Delta\rho_0 = 3$ veh/km, and $\Delta v_0 = 0.2l/\tau$, $\lambda_1 < \lambda_*$ is violated. Therefore, traffic is unstable. We solve the PW model under these initial conditions by using the implicit method with $N = 200$ and $K = 1600$. The solutions are shown in **Figure** 6. We can see from the figure that, for unstable initial conditions, a cluster traveling in a constant speed forms on the ring road. As we know, clusters cannot be observed from solutions of the corresponding LWR model. Instability that results in cluster solutions, therefore, is an important property of the PW model that distinguishes it from the LWR model. Detailed discussions of the structure and properties of cluster solutions can be found in (Jin and Zhang, 2001).

4.4 Simulation of traffic with lane-drops

In this subsection, we use the PW model to simulate traffic on a ring road with a bottleneck at $[320l, 400l]$:

$$a(x) = \begin{cases} 1, & x \in [320l, 400l), \\ 2, & [0, 320l) \text{ or } (400l, 800l], \end{cases}$$

where $a(x)$ is the number of lanes.

For the inhomogeneous roadway, the PW model can be modified as

$$\begin{pmatrix} \rho \\ q \end{pmatrix}_t + \begin{pmatrix} q \\ \frac{q^2}{\rho} + c_0^2\rho \end{pmatrix}_x = \begin{pmatrix} 0 \\ \frac{\rho v_*(\rho/a(x)) - q}{\tau} \end{pmatrix}. \tag{35}$$

Since the only difference of this model from (4) is the source term, the Godunov methods can be directly applied.

For the following initial traffic conditions,

$$\begin{aligned} \rho(x,0) &= a(x)(\rho_h + \Delta\rho_0 \sin\tfrac{2\pi x}{L}), \quad x \in [0, L], \\ v(x,0) &= v_*(\rho_h) + \Delta v_0 \sin\tfrac{2\pi x}{L}, \qquad x \in [0, L], \end{aligned} \tag{36}$$

in which $\rho_h = 20$ veh/km/lane, $\Delta\rho_0 = 3$ veh/km/lane, and $\Delta v_0 = 0.002$ km/s, solutions of the PW model as well as those of the corresponding LWR model are shown in **Figure** 7. (For detailed discussions for solving the LWR model for inhomogeneous roadways, please refer to (Jin and Zhang, 2000).) From the figure we can see that, for both models, a congested region forms upstream to the bottleneck and traffic flow-rate approaches constant after a sufficient long time. However, the constant flow-rate for the LWR model, which is capacity flow of one lane, is higher than that for the PW model.

5 Conclusions

In this paper, we studied first the Riemann problem of the homogeneous version of the PW model and then different numerical methods for solving the PW model. These methods combine a first-order Godunov-type approximation of the homogeneous version of the system and different treatments of the source term. They can replace many ad-hoc numerical methods for the PW model that do not fully make use of the property that the PW model is a hyperbolic system of conservation laws with relaxation.

From the numerical results, we can see that, when the PW model is stable, its solutions are close to those of the LWR model, and different numerical methods, including the implicit method, the explicit method, and the fractional step splitting method, produce similar results. We also show when the PW model is unstable, it is capable of simulating cluster effects in traffic. The PW model can also be applied without major modifications for inhomogeneous roadways.

References

[1] G.Q. Chen, C.D. Levermore and T.P. Liu, *Hyperbolic conservation laws with stiff relaxation terms and entropy*, Communications on Pure and Applied Mathematics, Vol. XLVII, pp. 787-830, 1994.

[2] R. Courant, K. Friedrichs and H. Lewy, *ber die partiellen differenzengleichungen der mathematischen physik*, Math. Ann. 100, pp. 32-74, 1928.

[3] S.K. Godunov, *A difference method for numerical calculations of discontinuous solutions of the equations of hydrodynamics*, Mat. Sb., 47, pp. 271-306, 1959. (In Russian.)

[4] M. Herrmann and B.S. Kerner, *Local cluster effect in different traffic flow models*, Physica A 255, pp. 163-198, 1998.

[5] W.L. Jin and H.M. Zhang, *The inhomogeneous kinematic wave traffic flow model as a resonant nonlinear system*, University of California at Davis, submitted to Transportation Science, 2000.

[6] W.L. Jin and H.M. Zhang, *The formation and structure of vehicle clusters in the Payne-Whitham traffic flow model*, submitted to Transportation Research B, 2001.

[7] B.S. Kerner and P. Konhäuser, *Structure and parameters of clusters in traffic flow*, Physical Review E, Vol. 50, No. 1, pp. 54-83, 1994.

[8] P.D. Lax, *Hyperbolic systems of conservation laws and the mathematical theory of shock waves*, SIAM, Philadelphia, Pennsylvania, 1972.

[9] C.J. Leo and R.L. Pretty, *Numerical simulation of macroscopic continuum traffic models*, Transportation Research B, Vol. 26, No. 3, pp. 207-220, 1992.

[10] M.J. Lighthill and G.B. Whitham, *On kinematic waves: II. A theory of traffic flow on long crowded roads*, Proc. Royal Society, Vol. 229 (1178) of A, pp. 317-345, 1955.

[11] T.P. Liu, *Quasi-linear hyperbolic systems*, Commun. Math. Phys. 68, pp. 141-172, 1979.

[12] T.P. Liu, *Hyperbolic conservation laws with relaxation*, Comm. Math. Phys., 108, pp. 153-175, 1987.

[13] H.J. Payne, *Models of freeway traffic and control*, in Mathematical Models of Public Systems, Vol. 1 of Simulation Councils Proc. Ser., pp. 51-60, 1971.

[14] R.B. Pember, *Numerical methods for hyperbolic conservation laws with stiff relaxation I. Spurious solutions*, Siam J. Applied Mathematics, Vol. 53, No. 5, pp. 1293-1330, 1993.

[15] P.I. Richards, *Shock waves on the highway*, Operations Research, Vol. 4, pp. 42-51, 1956.

[16] S. Schochet, *The instant response limit in Whitham's nonlinear traffic model: uniform well-posedness and global existence*, Asymptotic Analysis 1, pp. 263-282, 1988.

[17] J. Smoller, *Shock waves and reaction-diffusion equations*, New York, Springer-Verlag, 1983.

[18] G.B. Whitham, *Some comments on wave propagation and shock wave structure with application to magnetohydronamics*, Comm. Pure Appl. Math., Vol. XII, pp. 113-158, 1959.

[19] G.B. Whitham, *Linear and nonlinear waves*, John Wiley and Sons, New York, 1974.

[20] H.M. Zhang, *A theory of nonequilibrium traffic flow*, Transportation Research B, Vol. 32, No. 7, pp. 485-498, 1998.

[21] H.M. Zhang, *An analysis of the stability and wave properties of a new continuum theory*, Transportation Research B, Vol. 33, No. 6, pp. 387-398, 1999.

[22] H.M. Zhang, *Structural properties of solutions arising from a non-equilibrium traffic flow theory*, Transportation Research B, Vol. 34, pp. 583-603, 2000.

[23] H.M. Zhang, *A finite difference model of nonequilibrium traffic flow*, Transportation Research B, Vol. 35, No. 5, pp. 337-365, 2001.

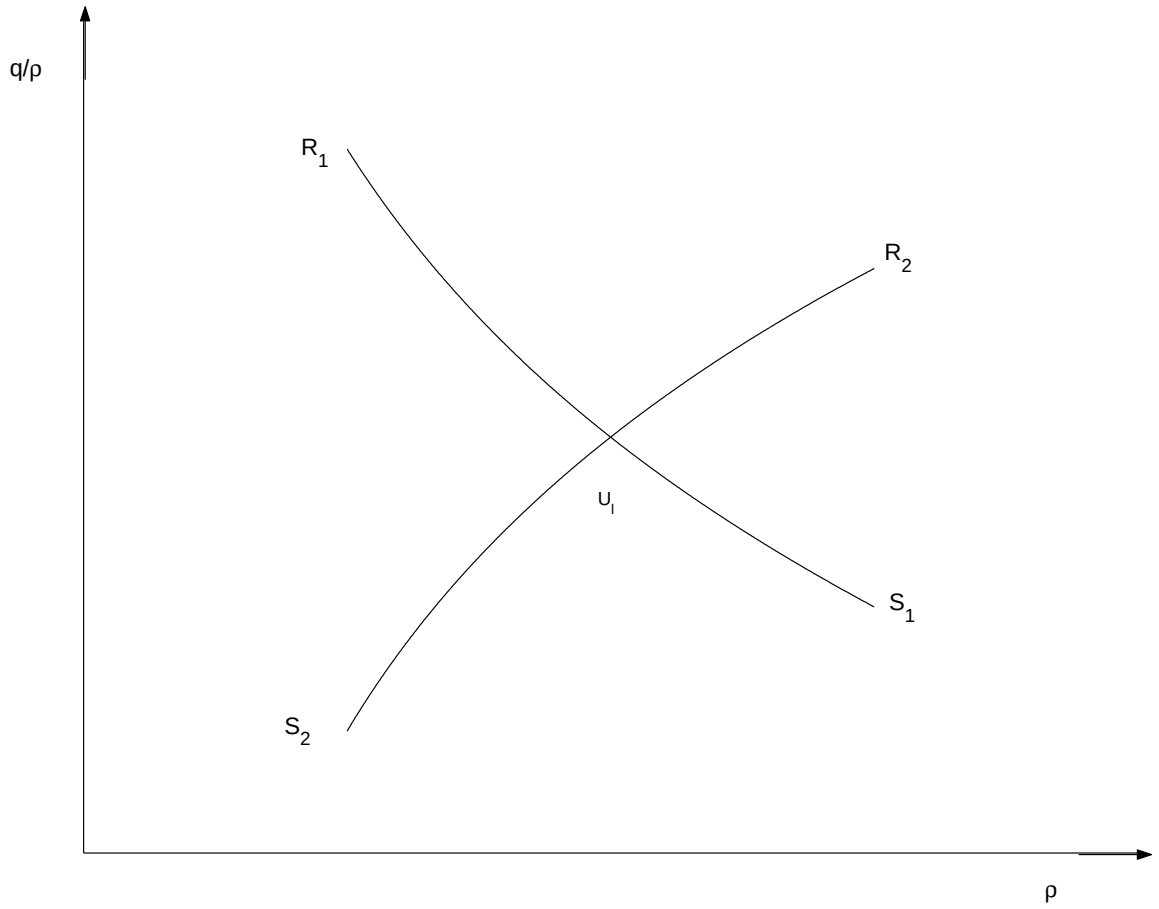

Figure 1: Basic curves in the $\rho - q/\rho$ plane

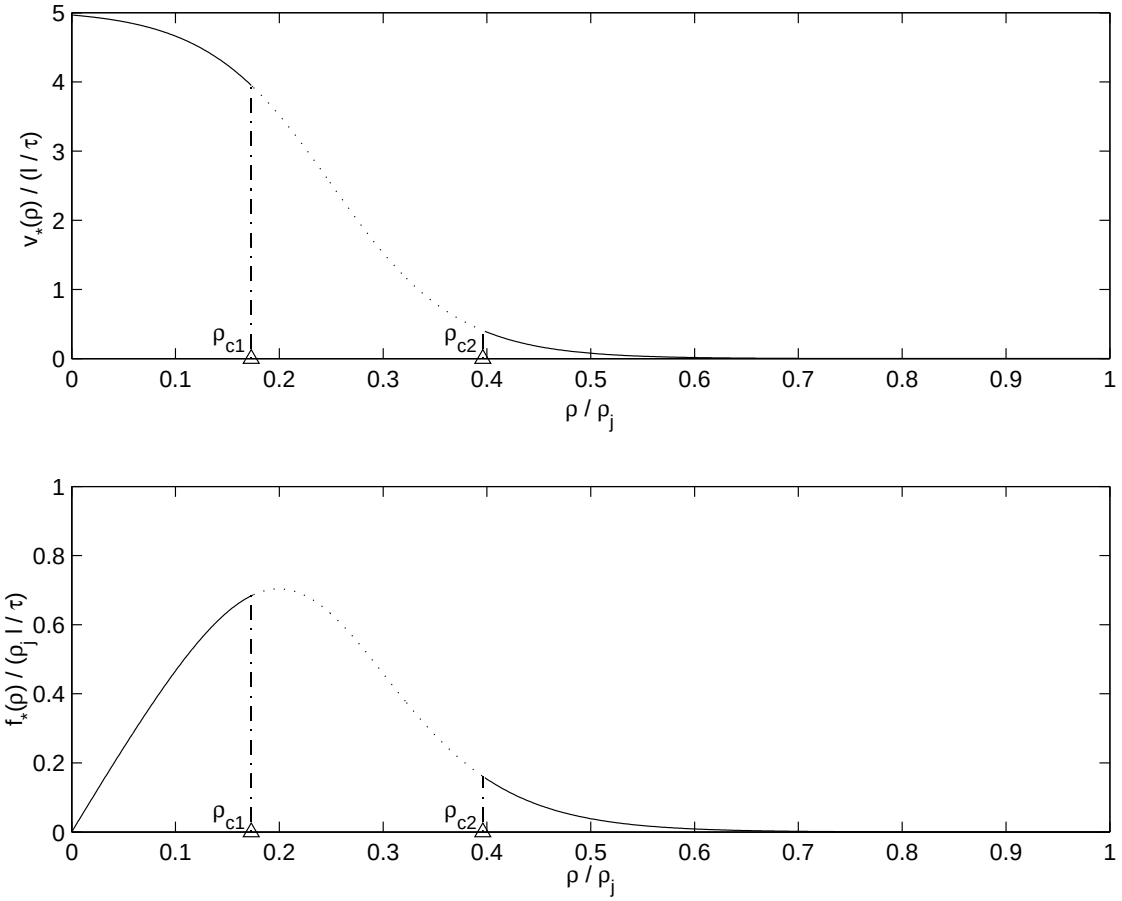

Figure 2: The Kerner-Konhäuser model of speed-density and flow-density relations

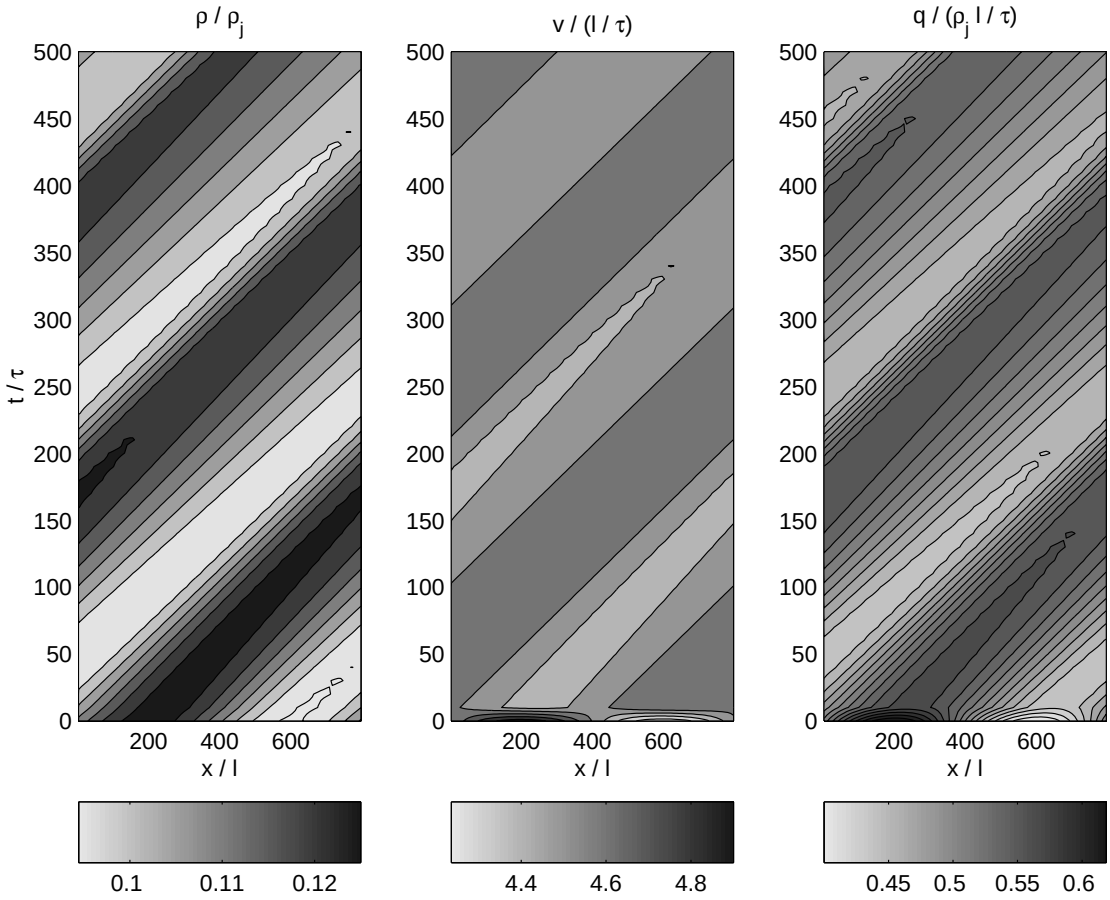

Figure 3: Solutions of the PW model by using the implicit method: $N = 100$ and $K = 500$

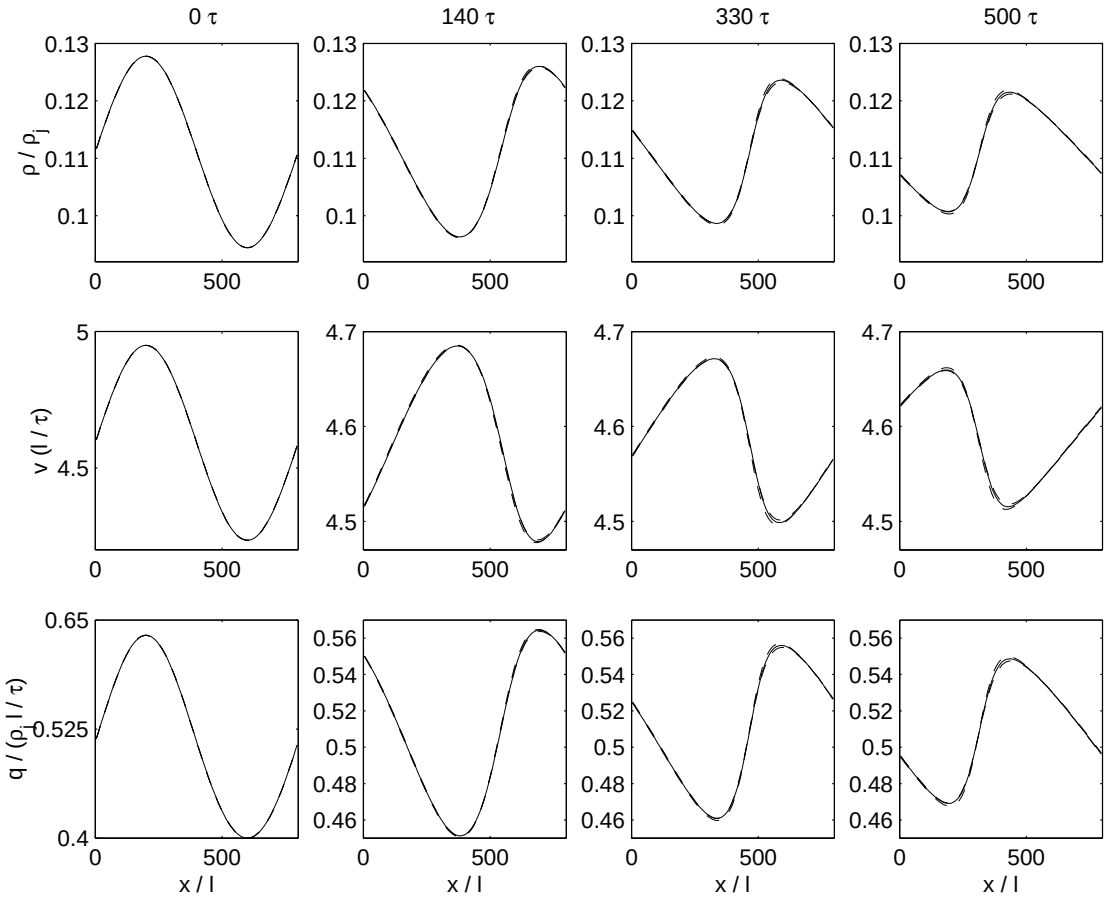

Figure 4: Comparison of solutions of the PW model with different methods: thinner solid lines for the implicit method, thinner dashed lines for the fractional splitting method, and thicker dashed lines for the explicit method

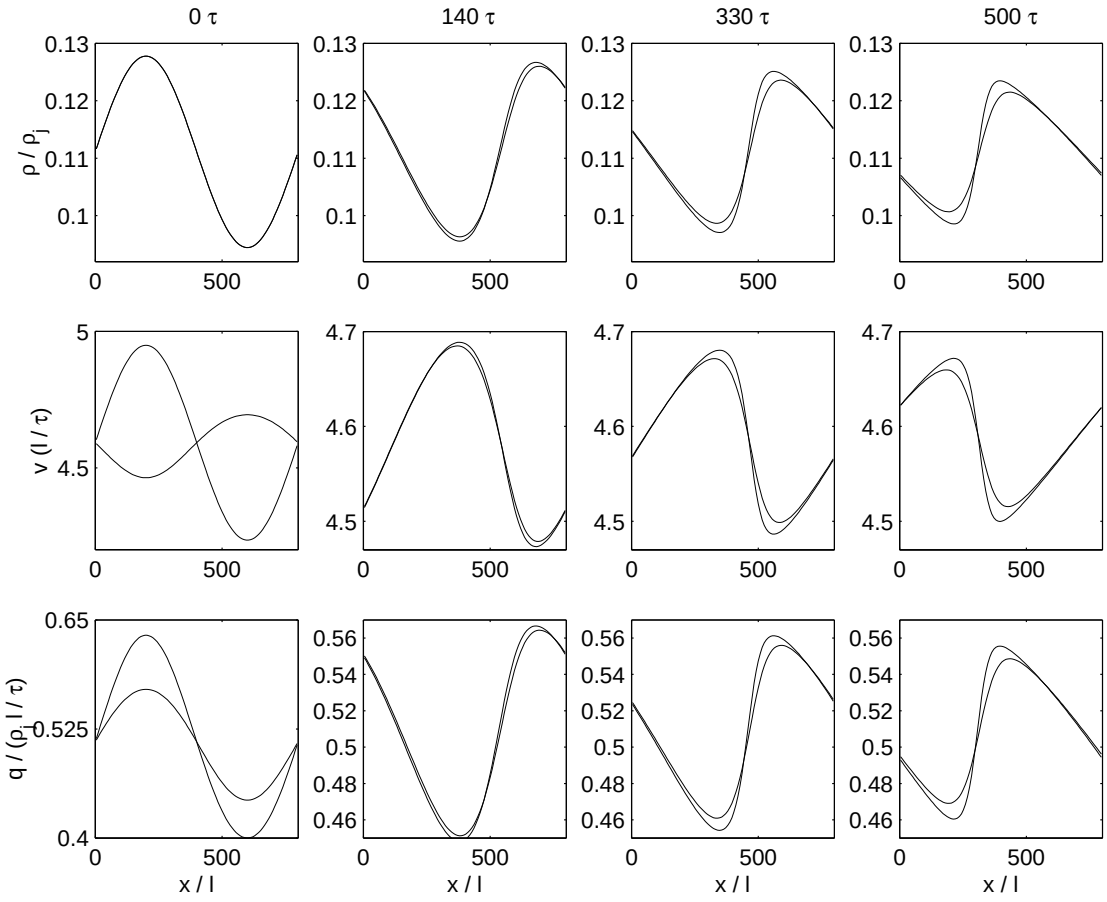

Figure 5: Comparison of solutions of the LWR and PW models on a homogeneous roadway: thicker lines for the LWR model and thinner lines for the PW model

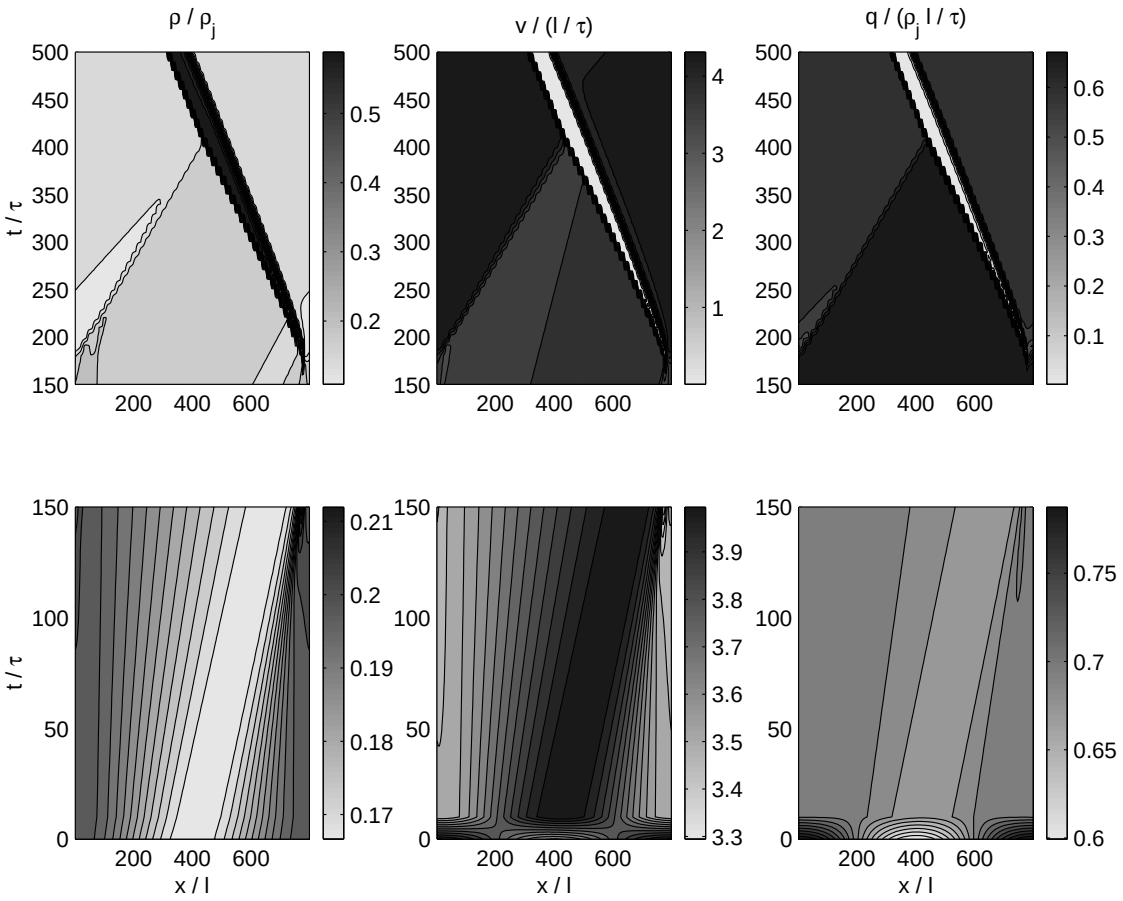

Figure 6: The formation of a cluster for initial condition (34)

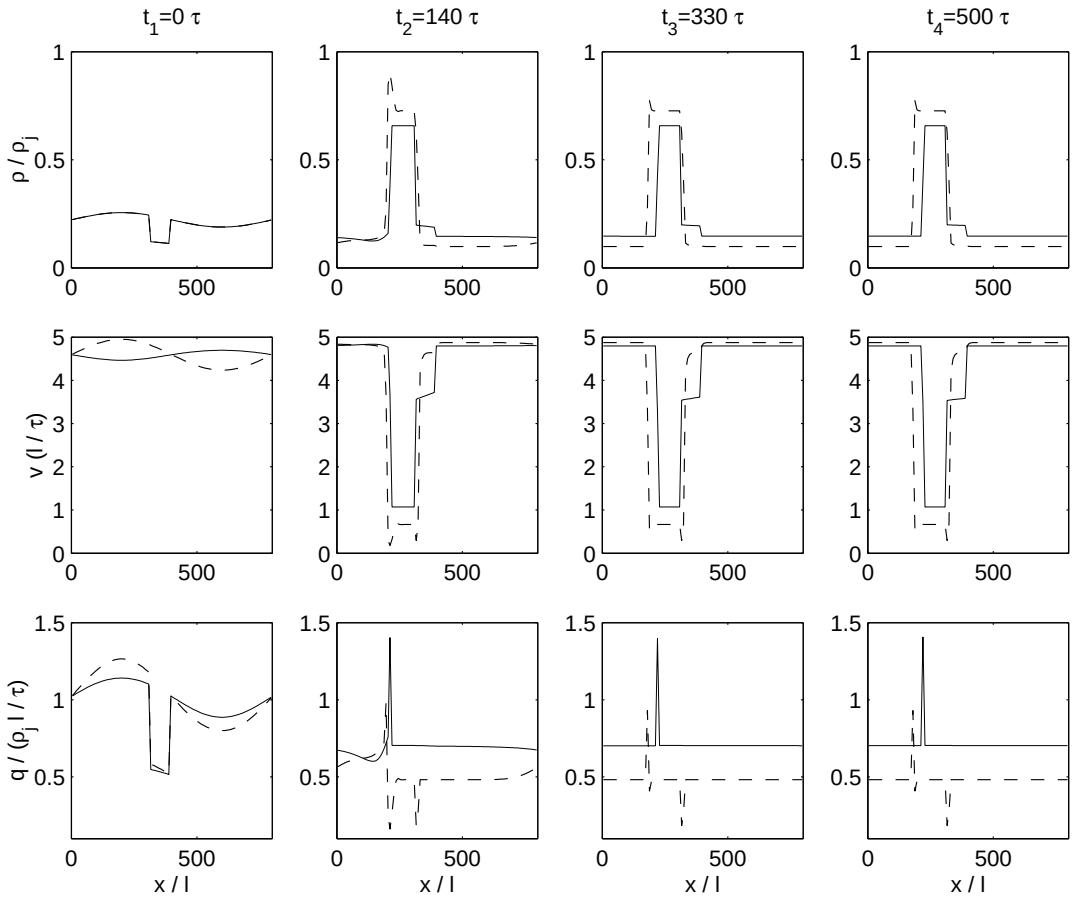

Figure 7: Comparison of solutions of the LWR and PW models on an inhomogeneous ring road: Solid lines for the LWR model and dashed lines for the PW model